

Mobility Evaluation of BTBT Derivatives: Limitation and Impact on Charge Transport

Robert Wawrzinek,^{a,b,†} Jan Sobus,^{a,b,†} Mujeeb Ullah Chaudhry,^{a,b} Viqar Ahmad,^{a,b} Arnaud Grosjean,^c Jack K. Clegg,^c Ebinazar B. Namdas^{a,b,*} and Shih-Chun Lo^{a,c,*}

^a Centre for Organic Photonics & Electronics, The University of Queensland, Brisbane, Queensland 4072, Australia

^b School of Mathematics and Physics, The University of Queensland, Brisbane, Queensland 4072, Australia.

^c School of Chemistry and Molecular Biosciences, The University of Queensland, Brisbane, Queensland 4072, Australia.

*Correspondence to: s.lo@uq.edu.au and e.namdass@uq.edu.au;

† RW and JS contributed equally.

Keywords: organic transistors, charge transport, mobility, organic electronics, BTBT

ABSTRACT

Amongst contemporary semiconductors many of the best performing materials are based on [1]benzothieno[3,2-b][1]benzothiophene (BTBT). Alkylated derivatives of these small molecules not only provide high hole mobilities but can also be easily processed by thermal vacuum or solution deposition methods. Over the last decade numerous publications have been investigating molecular structures and charge transport properties to elucidate what makes these molecules so special. However, the race towards ever higher mobilities resulted in significantly deviating values, which exacerbates linking molecular structure to electronic properties. Moreover, a recently arisen debate on overestimation of organic field-effect transistor mobilities calls for a reevaluation of these numbers. We synthesised and characterised four BTBT derivatives with either one or two alkyl chains (themselves consisting of either

eight or ten carbon atoms), and investigated their spectroscopic, structural and electrical properties. By employing two probes, gated 4-point probe and gated van der Pauw measurements, we compare field effect mobility values at room and low temperatures, and discuss their feasibility and viability. We attribute mobility changes to different angles between molecule planes and core-to-core double layer stacking of asymmetric BTBT derivatives and show higher mobilities in the presence of more and longer alkyl chains. A so called “zipper effect” brings BTBT cores in closer proximity promoting stronger intermolecular orbital coupling and hence higher charge transport.

INTRODUCTION

Semiconducting thienoacenes were first applied in organic field-effect transistors (OFETs) in the 1990s, albeit showing only moderate hole mobilities. In the mid-2000s, the first molecules based on [1]benzothieno[3,2-*b*][1]benzothiophenes (BTBT) gave unprecedented high mobilities of up to $2.0 \text{ cm}^2/\text{Vs}$, leading to an increasing interest in these structures ever since.¹ To date, the literature provides a plethora of examples of BTBT derivatives used as hole transport layers in OFETs, photo-transistors and organic light-emitting transistors (OLETs).²⁻⁶ Over the years, alkylated variants turned out to provide superior performances, with C₈-BTBT-C₈ as their most prominent representative.

As solution and vacuum deposition are feasible fabrication techniques, record-high mobilities of up to $50 \text{ cm}^2/\text{Vs}$ have been reported (a comprehensive selection of BTBT semiconductors and their reported OFET performances can be found in **Table S1** in the Supporting Information). However, it was just recently that a reconsideration regarding the determination of OFET charge mobility has caused many doubts in how to interpret values from different sources and how to derive structure-property relations from them.⁷⁻⁹

Transistor mobility calculation by conventional current-voltage equations strongly depends on device geometry and does not account for contact resistance caused by the presence of an injection barrier. The latter arises from an energetic mismatch between the charge injecting metal electrode and the organic semiconductor's energy level (*i.e.*, the highest occupied molecular orbital for p-channel transistors). Furthermore, polycrystalline films generally exhibit a high degree of disorder, evoked by varied chain length and angles, defects, voids and crystal boundaries. These factors in turn provoke inhomogeneous carrier mobilities at different carrier concentrations impeding reliable mobility calculations from simplistic MOSFET

current-voltage equations. Often, but not necessarily, overestimated mobilities were derived from *current* against *voltage* plotted measurements showing a “kink” between linear and saturation regime.⁹ A recent review provides in depth analysis of the impact of contact resistance and importance of protocols used for mobility extraction.¹⁰ Gated 4-probe measurements eliminate the issue of contact resistance but are geometry dependent.^{11,12} Also correct probe positioning and confinement of the organic layer are crucial to generate meaningful results and avoid overestimation.^{7,13} A third approach to mobility calculation is the gated van der Pauw method, which removes both of the above limiting factors (*i.e.*, geometry factor and contact resistance) and allows for feasible performance statistics, since a single device can be measured in eight different orientations.

In this article, we aim to provide a contemporary experimental comparison between the three above mentioned methods in the context of alkylated BTBT semiconductors. A recent theoretical study identified the restraining forces of longer alkyl chains ($C_n > 8$) to promote a herringbone arrangement, as compared to the π - π stacking of BTBT derivatives with shorter chains. The resulting increase in molecular order enables a strong/balanced intermolecular charge-transfer, as well as reduced electron-phonon coupling and consequently in high mobility BTBT semiconductors.¹⁴ Thus, we selected a set of molecules that form herringbone structures varying in two parameters – number of surface groups and length thereof. Those five molecules are shown in **Figure 1** and include the widely used and commercially available **C₈BTBT-C₈** as well as the parental **BTBT** as a benchmark. All molecules were synthesised, fully characterised and investigated under identical conditions (details are provided in the Supporting Information). We present structural and electronic properties based on crystal structures, XRD, AFM and the aforementioned mobility measurements at room and low temperatures, reaching 70 K. Mobilities are then discussed concerning reliable value extraction,

impact on charge transport mechanisms as well as structure property relationships of BTBT derivatives.

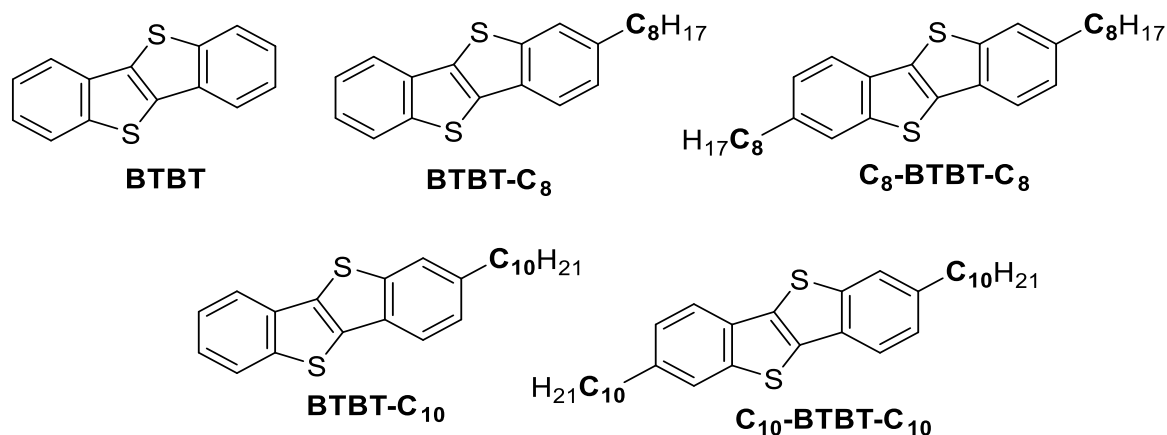


Figure 1. Molecular structures of parental, mono- and di-alkylated BTBTs (all alkyl chains are linear).

RESULTS AND DISCUSSION

Material synthesis:

All BTBTs reported here were synthesised following literature procedures.¹⁵⁻¹⁸ Detailed experimental procedures and characterization are described in the Supporting Information.

Spectroscopic properties of alkylated BTBT derivatives

Absorption and photoluminescence spectroscopy in toluene of the mono- and di-alkylated BTBT in this study show almost identical spectra, suggesting a marginal influence of the alkyl substitution on the chromophore (**Figure S1A** and **S1B** in Supporting Information). As expected, the length of the alkyl chains also does not affect the solution spectroscopic properties. However, when investigating evaporated thin films on quartz glass, the unique supramolecular order in BTBTs becomes evident and differences appear (**Figure S1C**): The solid state absorption spectra bathochromically shift with increasing number and length of the alkyl chain attached. It is also due to these long-range structures that accurate energetic

information on BTBTs (*e.g.*, ionization potentials, IPs) need to be derived from solid state rather than solution measurements.¹⁹ The photoluminescence spectra on the other hand seem to be less affected by those factors (**Figure S1D**).

Structural properties of alkylated BTBT derivatives

Figure 2 shows crystal structures of all BTBT derivatives. As mentioned before, the supramolecular order of BTBTs in solid state causes significant changes in the materials' properties when compared to those in solution. These long-range structures also massively contribute to charge transport in OFETs, hence, examination of crystal structures can help to gain insight in packing parameters that facilitate high transistor performance. Most fused thiophene containing semiconductors exhibit a herringbone packing, where side-by-side S...S(C) interactions overrule CH... π interaction of the aromatic rings, which otherwise would lead to a face-to-face orientation. The BTBT derivatives of this study are no exception and each molecule is surrounded by four edge-on and two off-set adjacent neighbours (**Figure 2**). This orientation can be enforced or disturbed by addition of surface groups. For instance, Ruzié *et al.* showed that alkoxy groups cause an offset between adjacent BTBT cores resulting in poor hole mobilities when employed in OFETs.¹⁹ Introduction of such functional moieties can polarise the chromophore's electron distribution. This increases π - π electronic repulsion, hence, forcing the molecules into a slipped-stacked packing.²⁰

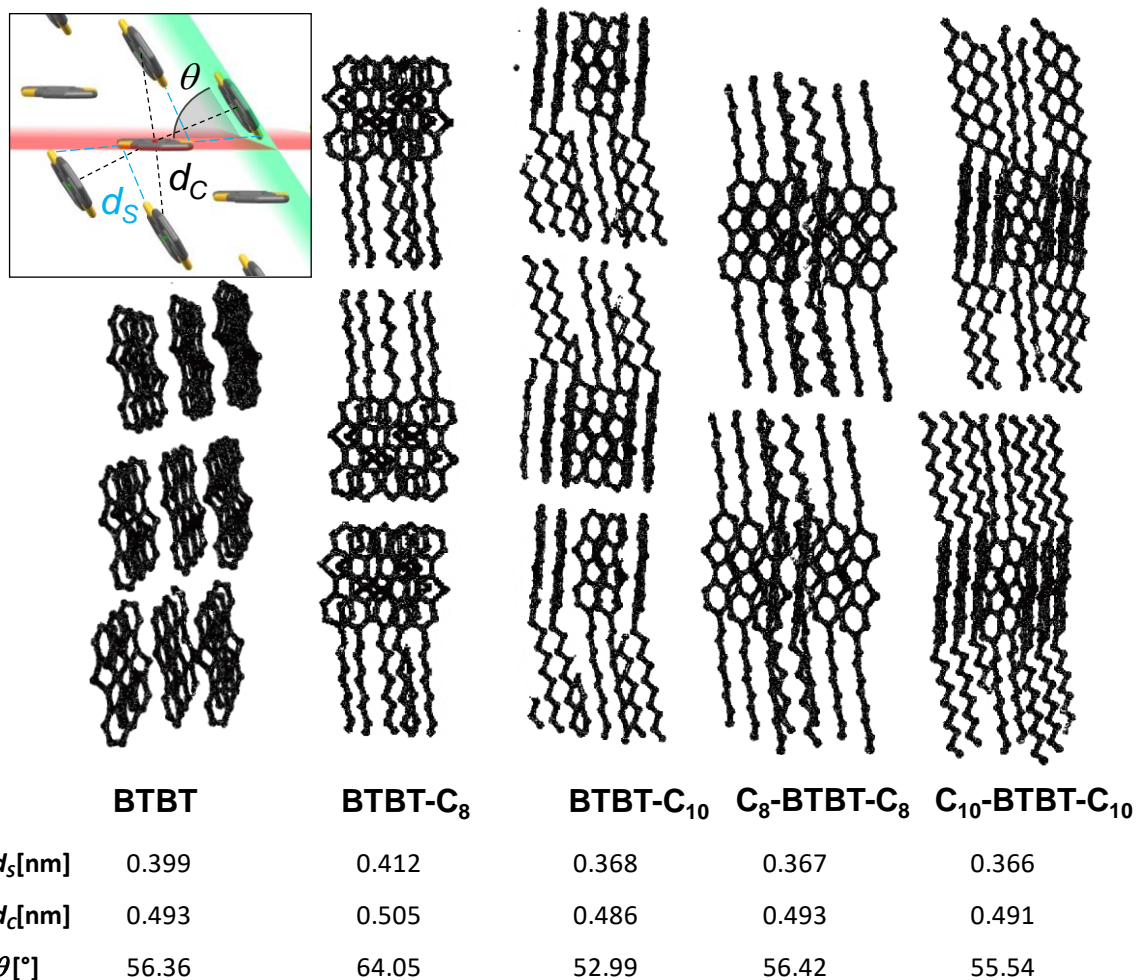


Figure 2. Herringbone packing of BTBTs (crystal structures of **BTBT**, **BTBT-C₈**, **C₈-BTBT-C₈** and **C₁₀-BTBT-C₁₀** were obtained from the literature).²¹⁻²³ d_s is the intermolecular distance between adjacent sulphur atoms that show relevant angles for potential orbital overlap, d_c is the distances between the four edge-on BTBT core centroids of each molecule and θ is the Herringbone angle between molecule planes.

Additionally to the edge-on packing observed in the parental BTBT, alkylated derivatives reduce the distance to their molecular neighbours due to the so called “zipper/fastener effect” induced by attractive dispersion forces.^{17,24,25} Minemawari *et al.* calculated higher interaction energies for increased alkyl-substituted BTBTs.²⁶ Alkan and Yavuz calculated that shorter alkyl chains in C_n-BTBTs-C_n (n = 3–5) exhibit strong π -stacking arrangements which tends to lean to a band-like transport. On the other hand, longer alkyl chains (n = 8, 10, 12) cause a herringbone arrangement, which can be better described by a hopping model.¹⁴ Interestingly,

when comparing distances between the four edge-on BTBT core centroids of each molecule (*d_c* **Figure 2 inset**), no general trend is observed. The proposed narrowing of the Herringbone angle θ is only apparent within the mono- or di-alkylated groups. However, the zipper effect brings sulphur atoms of edge-on neighbours in such close proximity that intermolecular orbital coupling is enabled.¹ This unique arrangement provides an unusual path for charges through the thin film – unlike most organic semiconductors, BTBT’s charge transport seems to take place perpendicular to the chromophores’ conjugated π -system.²⁵ It was suggested that the balance of π - π and tilted packing in BTBT molecules with herringbone arrangements is beneficial for charge transport.¹⁴ When calculating the intermolecular distance between adjacent sulphur atoms that show relevant angles for potential orbital overlap (*d_S* in **Figure 2 inset**), it becomes apparent that this value decreases with number and length of the alkyl chains. It is noted that this average distance of the parental **BTBT** (0.399 nm) is smaller than in case of **BTBT-C₈** (0.412 nm). Analysis of the X-ray diffraction (XRD) patterns of evaporated films (**Figure S2A**) provides more insight: Symmetric BTBT derivatives show main diffraction peaks that can be directly attributed to stacking molecule layers, with a calculated spacing close to the theoretical length of the molecule (**Figure S2B, Table S3**). Smaller peaks at higher angles appear at the integer multiplications of the main peak, showing higher orders of diffraction. However, for asymmetric BTBTs, the two tallest peaks appear at the spacing corresponding to single and double molecule length, indicating core-core double-layer stacking (as presented in **Figure 2**). Peaks of higher order appear as well but, as opposed to the doubly alkylated molecules, less pronounced. These results are supported by AFM images (**Figure S3** in the Supporting Information): For all compounds a layered, terrace-like structure is observed. While for the symmetric molecules the step height directly corresponds to the molecule length, in asymmetric BTBTs a step twice the molecule’s length is encountered much more frequently than the one corresponding to the single molecular layer. In addition, a longer alkyl chain (C₁₀

versus C₈) promotes higher surface roughness in both cases (mono- and di-alkylated), especially pronounced in the case of **BTBT-C₁₀**.

Mobility extraction:

This section will compare conventional two-probe, gated four-probe and gated van der Pauw mobility measurements. For each of the four BTBT derivatives, three types of devices (Transistor Transmission Line - TTL, Gated Four Point Probe -gFPP, Gated Van Der Pauw - gVDP) were prepared – the shared cross section can be seen in **Figure 3A**. All devices were manufactured on top of 0.5 mm thick Si wafer, acting as a substrate and gate electrode, covered with 400 nm of Si nitride acting as a dielectric layer. Additionally, a thin (~80 nm) polymethylmethacrylate (PMMA) layer was deposited on top of the nitride as a passivation layer, to minimize trapping at the dielectric-semiconductor interface. The total capacitance per unit area (C_l) value was equal to 12 nF/cm², which was calculated using PMMA thickness and dielectric constant and verified by LCR meter (Keysight E4980A). Next, 30 nm thick organic semiconductor layers were deposited using thermal evaporation through the shadow mask. They were followed by evaporation of contact electrodes consisting of 5 nm thick molybdenum oxide layer acting as a hole injecting layer and 35 nm gold layer. Shadow mask layouts (organic layer in red and contacts in blue) are presented in **Figure 3B-D** for TTL, gFPP and gVDP device architectures respectively. Thicknesses of the deposited layers were verified using DektakXT profilometer. Electrical characteristics were obtained using the Agilent B1500A semiconductor analyzer. Low temperature measurements were collected using the same device analyzer plugged to a Janis CCR12 cryogenic probe station cooled with Sumitomo HC-4E helium compressor system. The results of electrical measurements (exemplarily shown for **C₈-BTBT-C₈**) are presented in **Figure 3E–G**. Results for the other BTBTs are provided in the Supporting Information.

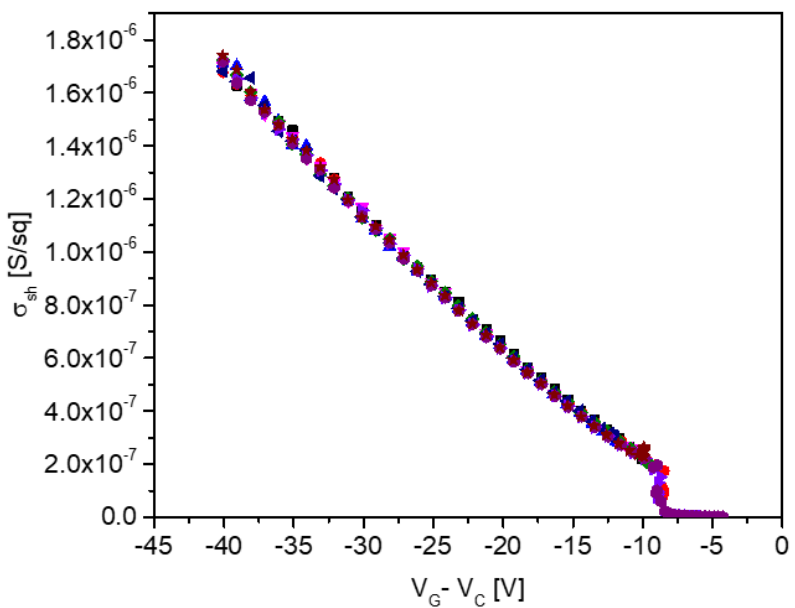
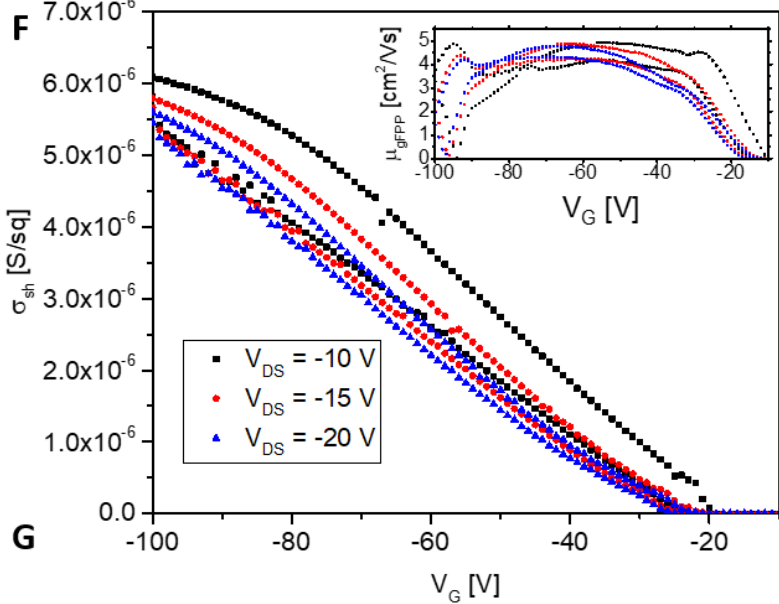
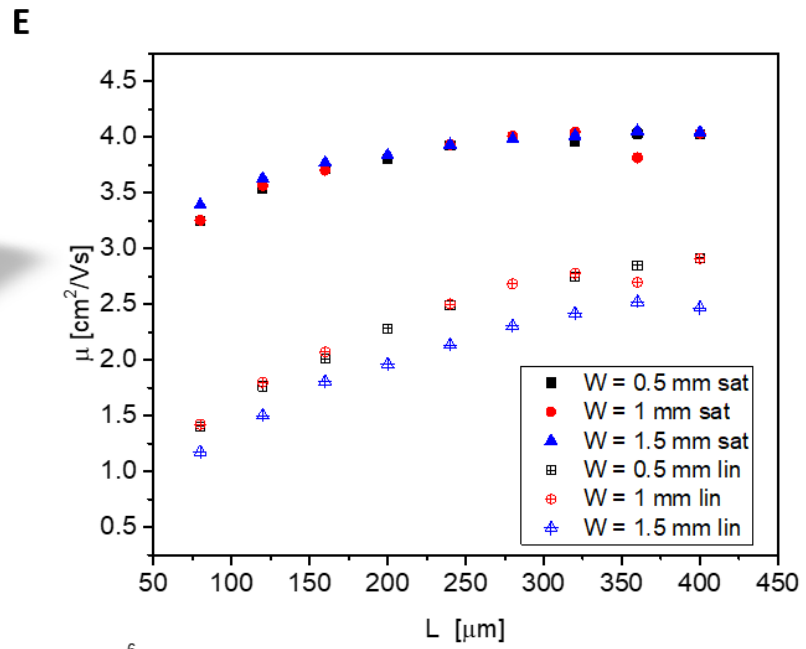
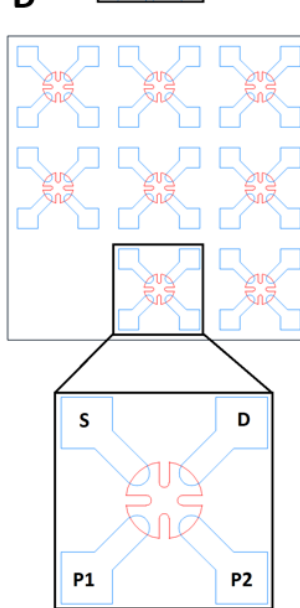
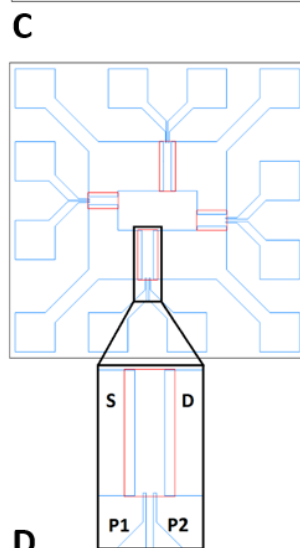
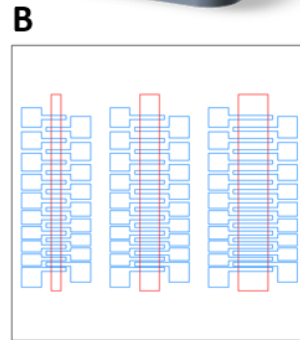
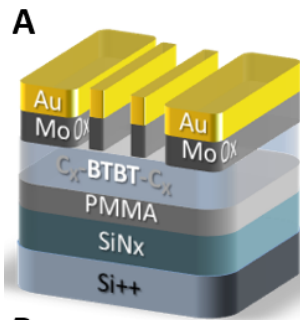


Figure 3. Shadow mask design employed in this study and mobility characteristics obtained for **C₈-BTBT-C₈** using three different techniques. Generalised cross-section of devices used in this study (A). Transistor transmission line (TTL) (B), gated Four Point Probe (gFPP) Method (C), gated van der Pauw (gVDP) Method (D). Linear (lin) and saturation (sat) mobility extracted from Transistor Transmission Line measurements for various channel widths and increasing length (E); conductivity plot for the gated four-point probe device for driven at varying source-drain voltages with the extracted mobility in the inset (F); gated van der Pauw conductivity plot combining eight measurements under different orientations for a single device (G).

Conventional two probe mobility measurements

Traditionally, the mobility of the OFET is extracted from their electrical characteristics by employing equations commonly used for the inorganic MOSFET devices:

$$I_{SD} = \frac{W}{L} \mu C_I \begin{cases} (V_G - V_T - \frac{1}{2} V_D) V_D & \text{when } V_D < (V_G - V_T) - \text{linear regime} \\ \frac{1}{2} (V_G - V_T)^2 & \text{when } V_D > (V_G - V_T) - \text{saturation regime} \end{cases} \quad (1)$$

Here, I_{SD} is the source-drain current density, W is channel width, L is channel length, μ is the charge carrier mobility, C_I is the capacitance per unit area, V_D and V_G are the bias voltages of the drain and gate electrodes respectively and the source electrode is grounded, $V_S = 0$. While these equations do not take into account the subthreshold behaviour or electric field degradation of mobility (as more sophisticated models do).²⁷ However, their results are still sufficient for a general evaluation of channel material performance. Usually, transfer characteristics $I_{SD}(V_G)$ (swipe at fixed V_D - low V_D for linear mobility, high V_D for saturation mobility) are measured and then, based on equation (1), the mobility is extracted from the slope of I_{SD} versus V_G or $\sqrt{I_{SD}}$ versus V_G for linear and saturation regimes, respectively. However, this approach has two fundamental flaws. First, it does not take into account the contact resistances present in the device (which come from the electrodes, electrode-material interface or even the vertical transport in the material itself), thus lowering the obtained mobility value. Second, the obtained mobility value strongly depends on the geometric factor L/W . Small variation in one or both of

those parameters (especially channel length L , which usually is in the range of tens of microns) can lead to significant error in the obtained mobility value. The nature of the contacts itself (Ohmic or Schottky type) and the resulting deviation from those ideal equations can lead to errors in several orders of magnitude, as has been described in detail elsewhere.⁹ Therefore, we describe in the following three measuring methods we employed in order to evaluate the BTBT derivatives, which mitigate one or both of these problems.

Transistor transmission line (TTL) method

One of the ways of estimating the impact of the contact resistance is performing the series of mobility measurements on transistors with changing channel length L by keeping the channel width W constant (exemplarily shown in **Figure 3E**). **Figure 3B** shows three organic zones comprising of transistor widths of 0.5 mm, 1 mm and 1.5 mm (red colour) to create transistor transmission lines with channel lengths ranging from 80 μm to 400 μm (the blue colour indicates alternating electrodes). Typical transfer characteristics obtained from those devices are shown in the Supporting Information of **Figure S5**. Assuming the total resistance of the device being the sum of constant contact resistance and channel resistance varying with length (2), one can quickly derive that the extracted apparent mobility will be lower than the intrinsic mobility (3).^{7,28} This deviation will be particularly high for short channel length devices. With the increase of L , the measured mobility converges to the “true” value. Based on the series of measurements, both the contact resistance and true mobility can be estimated.

$$R_{tot}W = R_CW + \frac{L}{\mu_{true}C_I|V_G - V_T|} \quad (2)$$

$$\mu_{meas} = \mu_{true} \frac{1}{1 + R_C \frac{W}{L} \mu_{true} C_I |V_G - V_T|} \quad (3)$$

Where R_c and R_{tot} is contact and total resistance respectively. Although this method does not eliminate W and L dependence of the obtained results in terms of the absolute mobility value,

the number of devices produced on a single substrate provides a nice statistical picture. Detailed results for the remaining alkylated BTBTs can be seen in **Figure S6A, S7A and S8A**. As expected, the mobility from the TTL experiment increases with increasing channel length, both in linear and saturation regimes. The saturation mobility for **C₈-BTBT-C₈** showed the highest (4.1 cm²/Vs) and **BTBT-C₈** the lowest mobility value (0.3 cm²/Vs). Interestingly, the longer alkyl chain of **BTBT-C₁₀** tends to give higher mobilities in both the linear and the saturation region. Also, di-alkylated BTBT derivatives yielded higher mobility than their single-sided counterparts.

Gated four-point probe (gFPP) method

The four-point probe method for measuring conductivity was first used more than a century ago.¹¹ By introducing two additional voltage probes between source and drain electrodes in the current channel, one can entirely eliminate the influence of contact resistance. It is no surprise that this technique was soon implemented for mobility measurements in field-effect devices as a *Gated Four Point Probe* method, where the mobility is given by (4).

$$\mu_{true} = \frac{1}{C_I} \frac{\partial \sigma}{\partial V_G} \text{ where } \sigma = \frac{I_{SD}}{|V_1 - V_2|} \frac{D}{W} \quad (4)$$

Here, D is the distance between the voltage probes and V_{P1} and V_{P2} are their respective potentials. However, this method also has its drawbacks as it is even more prone to geometry errors and requires precise dimension values of all electrodes and distances between them. Moreover, when designing such an experiment, the L/W ratio should be kept as low as possible to avoid mobility overestimation. In order to prevent channel shunting, this also holds true for the width of the probes.²⁹ Furthermore, the organic layer itself should be confined to the area between source and drain to avoid mobility overestimation.¹³ Based on those considerations, we designed the electrode arrangement shown in the inset of **Figure 3C** with four different devices on each substrate ($W = 2500 \mu\text{m}$, $L = 400 \mu\text{m}$; $W = 2500 \mu\text{m}$, $L = 600 \mu\text{m}$; $W = 1500$

μm , $L = 400 \mu\text{m}$; $W = 1500 \mu\text{m}$, $L = 600 \mu\text{m}$) and narrow ($60 \mu\text{m}$ wide) voltage probes. Here, the red and blue colours represent the organic layer and the metal electrodes, respectively.

Figure 3F shows the sheet conductivity *versus* gate bias exemplarily for **C₈-BTBT-C₈** with three different source-drain voltages ranging from -10 V to -20 V . One can observe slight hysteresis in the obtained curves (especially for lower V_{DS}) and dips in mobility for very small and very large gate voltages. Yet, for the gate voltages ranging from -30 to -90 V , the mobility value remains stable and flat. Corresponding plots for the remaining BTBT derivatives can be found in the Supporting Information (**Figures S6B, S7B and S8B**). While the symmetric BTBTs show values well agreeing with the results from TTL measurements (mobility around $4 \text{ cm}^2/\text{Vs}$), the plots obtained for the mono-alkylated BTBT derivatives deviate significantly from linearity and are therefore not reliable for determination of a single value of mobility. Even after deriving the mobility from the steepest slope of the plot, the values remain lower (around $1 \text{ cm}^2/\text{Vs}$) than the ones for the di-alkylated counterparts.

Gated van der Pauw (gVDP) method

Important generalization of the four point probe method for conductivity measurements have been proposed by van der Pauw in the 1950s.^{30,31} By using the appropriate “clover-like” shape of the organic layer, one can change the geometric factor L/W into a constant value of $\ln(2)/\pi$. Moreover, the four-fold symmetry of the device allows eight different measurement orientations, which can detect any possible anisotropy (if present) in the sample, thus providing more data for averaged performance. Lately, a gated version of the van der Pauw method has been applied as a measuring tool for organic semiconductor layers with excellent results.³² The arrangement of electrodes used in this experiment is given in the inset of **Figure 3D**. Here, the red and blue colours represent the organic layer and the metallic electrodes, respectively.

During the measurement, a constant current flow is maintained between source and drain electrode (chosen as any pair of adjacent electrodes) by the source-drain bias. While the gate voltage is changed, source-drain bias changes accordingly to maintain the current. Source-drain bias and the biases on the two other electrodes acting as voltage probes V_{P1} and V_{P2} are monitored. This is exemplarily shown for **C₈-BTBT-C₈** in **Figure 3G**, where differently coloured points correspond to eight different electrode/current flow orientations. No directional or geometric dependence in the obtained results was observed. Subsequently, the sheet conductivity can be calculated using equation (5), which leads to extraction of mobility values by (6).

$$I_{SD} \frac{\ln(2)}{\pi} = \sigma_s |V_{P1} - V_{P2}| \quad (5)$$

$$\sigma_s = \mu_{true} C_I |V_G - V_T - V_C| \text{ where } V_C = \frac{V_{P1} + V_{P2}}{2} \quad (6)$$

Here, I_{SD} is the (constant) source-drain current, C_I is the capacitance per unit area of the dielectric layer, V_G is the applied gate potential, V_T is threshold voltage and μ_{true} is the extracted mobility. The obtained mobility value should be constant with changing source-drain currents (**Figure S4A**). From the obtained characteristics, it is also possible to easily distinguish between the linear and saturation regime (**Figure S4B**). The extracted mobility for **C₈-BTBT-C₈** reaches up to 4.2 cm²/Vs, which is close to the value obtained by the other two methods (**Figure 3E and 3F**). Corresponding plots for the remaining BTBT derivatives can be found in the Supporting Information (**Figures S6C, S7C and S8C**). Owing to the elimination of both major problems connected with mobility measurements – geometry dependence and impact of contact resistance – we consider the gated van der Pauw method to be the most reliable for measurements of mobility in organic thin films.

Correlating mobility with molecular structure

The mobility values collected by the three methods are summarised in **Table 1**: It shows that doubly-alkylated BTBTs are in general performing better than their mono-alkylated counterparts and that molecules with a shorter (-C₈) alkyl chain give more reproducible results. The first observation can be attributed to the core to core stacking in case of mono-alkylated molecules (as confirmed by XRD and AFM), which provides a “sideway” pathway for hole transport. In addition, **BTBT-C₈** exhibited a significantly larger herringbone angle and distance between molecules within a single plane than the other three compounds. This seems to be the defining factor behind its generally lower performance. The smaller dihedral angle of the **BTBT-C₁₀** enables higher mobility values, however, albeit having a quite low film quality (surface roughness of 12.6 nm). On the other hand, both bi-alkylated BTBTs show fairly consistent results with mobilities of similar magnitude. The slightly better result uniformity of **C₈-BTBT-C₈** (when compared to **C₁₀-BTBT-C₁₀**) can be attributed to better film quality (low surface roughness of ~2 nm, less grainy surface with larger domains). Our results confirm that **C₈-BTBT-C₈** is rightfully the BTBT derivative of choice in industry standards.

Table 1. Comparison of mobility values obtained for different BTBT derivatives using transistor transmission line (TTL), gated Four Point Probe (gFPP) and gated van der Pauw (gVDP) methods. (LIN = linear regime; SAT = saturation regime).

Material	$\mu_{\text{TTL (LIN)}}$ (cm²/Vs)	$\mu_{\text{TTL (SAT)}}$ (cm²/Vs)	μ_{gFPP} (cm²/Vs)	μ_{gVDP} (cm²/Vs)
BTBT-C₈	0.2±0.05	0.3±0.05	1.4±0.3*	0.4±0.05
BTBT-C₁₀	0.4±0.05	1±0.05	0.8±0.3*	2.7±0.1
C₈-BTBT-C₈	2.5±0.2	4.1±0.1	4.3±0.2	4.2±0.1
C₁₀-BTBT-C₁₀	1.3±0.1	3.8±0.2	3.3±0.2	4.3±0.1

* gFPP values for mono-alkylated BTBT derivatives are most likely over-estimated due to the leakage current overwhelming the source-drain current for those samples (see **Figures S7B** and **S8B** in the Supporting Information).

Understanding the charge transport mechanism – low temperature (T) measurements.

In order to understand the charge transport mechanism within the BTBT derivatives, we performed temperature dependent mobility measurements for gVDP devices (**Figure 4**).

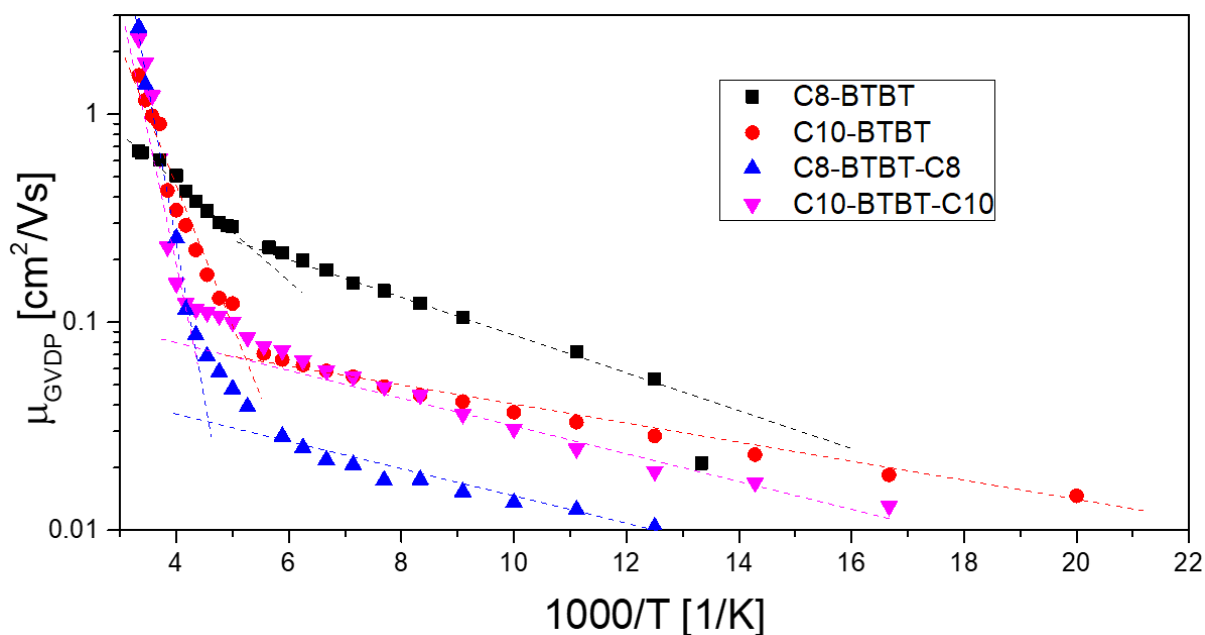


Figure 4. Mobility values obtained from gVDP devices for different BTBT derivatives plotted as a function of inverse temperature. Dotted lines are added as guide to the eye indicating transition between two mobility regimes (steeper for better conducting compounds).

It becomes apparent that the mobility's temperature dependence in these devices does not follow an Arrhenius-like behaviour. Instead, there are two distinct mobility regions – a high T region where the mobility is strongly temperature dependent and a low T region where it is almost independent. Such behaviour has been previously observed in OFETs and explained as a result of several phenomena including metal-to-insulator transition,^{33,34} Fowler-Nordheim tunneling³⁵ or a Luttinger liquid transport model.³⁶ As the curves from **Figure 4** are similar in shape for all BTBT derivatives, we chose **C₈-BTBT-C₈** as a model system to study the underlying transport mechanism in these compounds. First, we fabricated devices with three different thicknesses (10, 20, and 30 nm) of **C₈-BTBT-C₈** to confirm that vertical charge transport from the electrode contact towards the conductive channel is not the limiting factor, as it has been shown for high-mobility epitaxial devices.³⁷ From **Figure S9** in the Supporting

Information, one can see that such thickness modifications virtually cause no difference in device performance.

Next, output characteristics for the 20 nm device were measured for temperatures ranging from 300 K down to around 80 K, enabling the three dimensional analysis (T , V_{SD} , V_G). We plotted the obtained channel conductivity as a function of $T^{-1/2}$ for different gate and source drain biases (**Figure 5**). A transition between two conductivity regimes, similar to the situation in **Figure 4**, can be seen on these plots: At high V_{SD} bias (corresponding to a high electric field in the channel), the transition point between the two regimes has fixed temperature and is independent on the gate bias. However, upon moving to smaller source-drain voltages, this transition point shifts to lower temperatures (higher $T^{-1/2}$), up to a point where it is not visible anymore. It also becomes more dependent on the gate bias V_G (as can be seen especially for $V_{SD} = -3$ V). Such behaviour has been explained in detail by Bourbie *et al.*,³⁸⁻⁴⁰ who showed that the temperature dependence of DC conductivity in the 1D transport regime is given by equation (7), where T_1 is given by (8). Here, (l/α) corresponds to the localization length (that can be changed with V_G via Fermi level shift), N is density of states and k_B is the Boltzmann constant. The critical temperature T_c , which separates two conductivity regimes, is field dependent and given by (9). Here, e is the electron charge and E is the electric field in the channel (being proportional to V_{SD}). There also exists the critical electric field E_C , corresponding to the energy state bandwidth Δ as $eE_C R = \Delta$ (with R being the distance between the hopping sites). It puts the limitation on the maximum critical temperature $T_C(E_C) = \Delta/2\alpha k_B R$.

$$\sigma(T) = \sigma_0 \exp\left(-\sqrt{\frac{T_1(E)}{T}}\right) \quad (7)$$

$$T_1(E) = \frac{4\alpha}{k_B N} \left[1 - \frac{T_C(E)}{T}\right] \quad (8)$$

$$T_C(E) = eE/2 \alpha k_B \quad (9)$$

Figure 6 presents compiled T_c and slopes of conductivity curves in both regimes. As predicted by equations (7–9), the critical temperature mildly increases with the increased gate bias (and thus localization length). At first sight, there seem to be no V_{SD} dependence, at least at high voltages. This steady behaviour is governed by staying in the regime over the critical electric field. Yet, as soon as the field in the channel drops below the critical value (in our geometry achieved at around 3V), the associated T_c rapidly drops and the transition can no longer be detected by our setup (both due to the very small signals and low temperature).

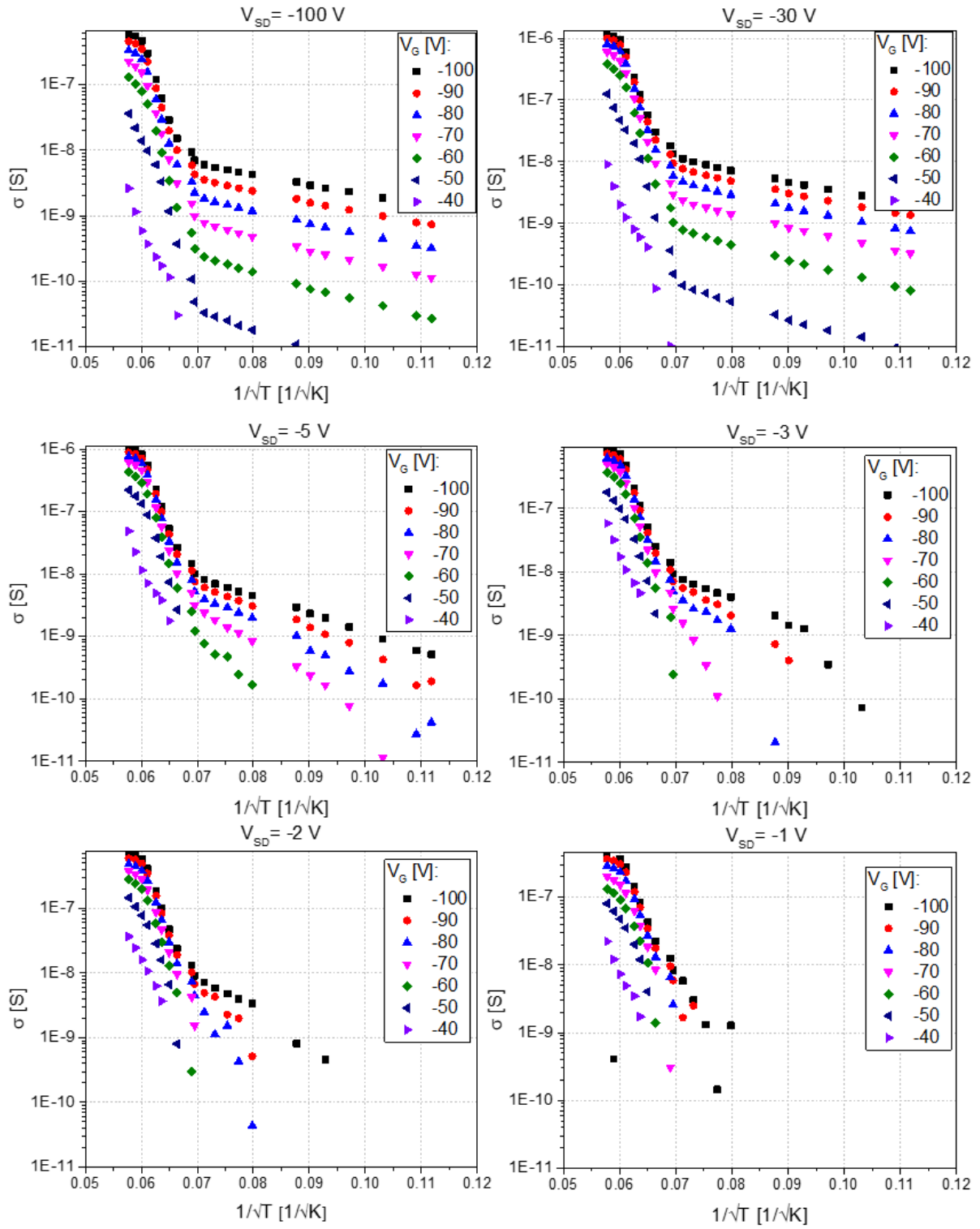


Figure 5. Channel conductivity for a 20 nm thick C_8 -BTBT- C_8 device plotted as a function of temperature, source-drain bias (corresponding to electric field across the channel) and the gate voltage.

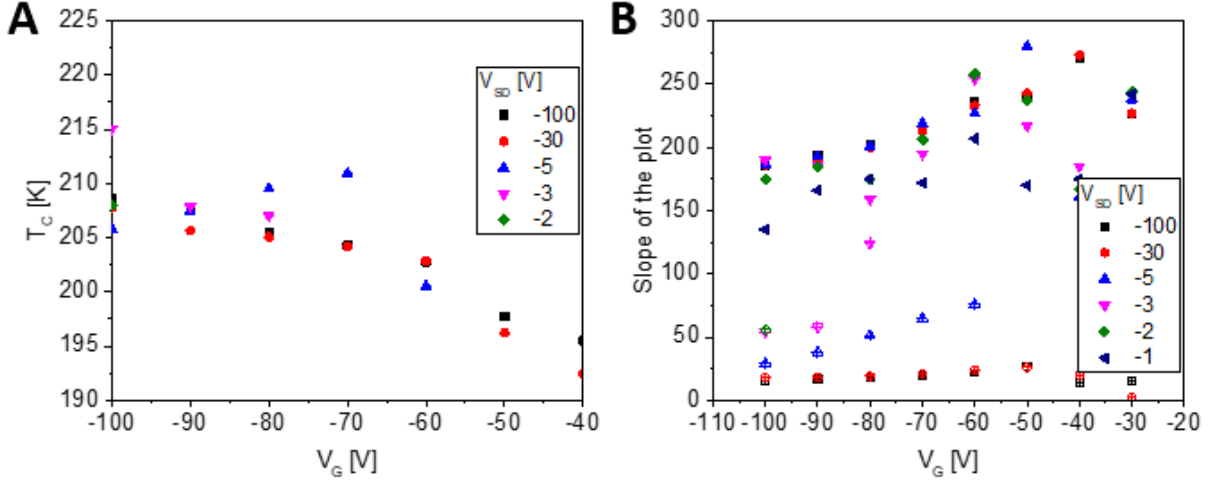


Figure 6. Critical temperature extracted from **Figure 5** plotted as a function of gate bias for different source-drain voltages (**A**); conductivity slope from **Figure 5** in the two regimes – over the T_c (full spots) and below T_c (crossed spots) for varying V_G and V_{SD} (**B**).

In the case of $T < T_c$, the tunnelling process (phonon-emission) takes over and T dependence is reduced significantly. Now, the $\ln \sigma$ should be proportional to $E^{-1/2}$, which is the situation in **Figure S10** (Supporting Information). Here we used V_{SD} as it is proportional to E , and only small deviation from linearity is observed at lower gate voltages and/or very low V_{SD} . We also excluded the possibility of transition from a rectangular to triangular energy barrier shape, also known as Fowler-Nordheim tunnelling (FN). Plotting $\ln(I_{SD}/V_{SD}^2)$ as a function of $1/V_{SD}$ can give a clear indication on the barrier type.³⁴ Expressions for the rectangular (10) and triangular (11) barriers are given below.

$$\ln\left(\frac{I_{SD}}{V_{SD}^2}\right) \propto \ln\left(\frac{1}{V_{SD}}\right) - \frac{2d\sqrt{2m}\phi}{\hbar} \quad (10)$$

$$\ln\left(\frac{I_{SD}}{V_{SD}^2}\right) \propto -\frac{4d\sqrt{2m}\phi}{3\hbar q} \left(\frac{1}{V_{SD}}\right) \quad (11)$$

We provide FN plots for the 20 nm **C₈-BTBT-C₈** device obtained for different temperatures in the Supporting Information of **Figure S11**. In all cases, the curves show logarithmic shapes, indicating a rectangular potential barrier.

CONCLUSIONS

In summary, we investigated a set of symmetrically and asymmetrically alkylated BTBT derivatives and correlated their structural differences to OFET performance. By using different mobility measurement techniques, we observed higher hole mobilities in molecules with symmetric alkylation, assigned to induction of a “zipper effect” which brings sulphur atoms of adjacent BTBT cores in closer proximity. As a result, an increase in intermolecular orbital coupling provides charge transport perpendicular to the plane of the chromophores’ conjugated π -system and along the FET channel. In addition, alkyl chains on both sides of BTBT core prevent core-core stacking, thus creating a more beneficial charge transport pathway. The Gated van der Pauw method was found to be the most reliable technique for measuring FET mobility: It eliminates both impact of the contact resistance and errors coming from geometry dependence of other methods, whilst providing statistical information for a single sample. This method gave very comparable mobility values of 4.2 and 4.3 cm^2/Vs for **C₈-BTBT-C₈** and **C₁₀-BTBT-C₁₀**, respectively, and much lower values of 0.4 and 2.7 cm^2/Vs for their mono alkylated counterparts. However, it is worth noting that longer (C₁₀) alkyl chains result in reduced film quality. Finally, we applied a compact model of conductivity, including temperature and field based transitions between different conductivity regimes to explain non-Arrhenius temperature dependence of the measured mobility in these materials.

ACKNOWLEDGEMENTS

We thank the Australian Research Council (ARC) for financial support (ARC DP140101088 and ARC DP160100700) and Department of Industry, Innovation and Science (AISRF53765) for financial support. E.B.N. is the recipient of a UQ Fellowship. V.A. was funded by an Australian Postgraduate Award. This work was performed in part at the Australian National

Fabrication Facility Queensland Node (ANFF-Q), a company established under the National Collaborative Research Infrastructure Strategy to provide nano- and microfabrication facilities for Australia's researchers.

SUPPORTING INFORMATION

Material synthesis procedures, photophysical spectroscopy, XRD, AFM, and electrical measurements are provided in the accompanying Supporting Information.

REFERENCES

- (1) Takimiya, K.; Osaka, I.; Mori, T.; Nakano, M. Organic Semiconductors Based on [1]Benzothieno[3,2-b][1]Benzothiophene Substructure. *Acc. Chem. Res.* **2014**, *47*, 1493–1502.
- (2) Ullah, M.; Wawrzinek, R.; Maasoumi, F.; Lo, S.-C.; Namdas, E. B. Semitransparent and Low-Voltage Operating Organic Light-Emitting Field-Effect Transistors Processed at Low Temperatures. *Adv. Opt. Mater.* **2016**, *4*, 1022–1026.
- (3) Generali, G.; Soldano, C.; Facchetti, A.; Muccini, M. Innovative Trilayer Organic Light Emitting Transistor (OLET) Structure for Blue Emission. *SID Symp. Dig. Tech. Pap.* **2016**, *47*, 1779–1782.
- (4) Liu, X.; Luo, X.; Nan, H.; Guo, H.; Wang, P.; Zhang, L.; Zhou, M.; Yang, Z.; Shi, Y.; Hu, W.; Ni, Z.; Qiu, T.; Yu, Z.; Xu, J.-B.; Wang, X. Epitaxial Ultrathin Organic Crystals on Graphene for High-Efficiency Phototransistors. *Adv. Mater.* **2016**, *28*, 5200–5205.
- (5) Ullah, M.; Wawrzinek, R.; Maasoumi, F.; Lo, S.-C.; Namdas, E. B. UV-Deep Blue-Visible Light-Emitting Organic Field Effect Transistors with High Charge Carrier Mobilities. *Adv. Opt. Mater.* **2017**, *5*, 1600973.
- (6) Prosa, M.; Benvenuti, E.; Pasini, M.; Giovanella, U.; Bolognesi, M.; Meazza, L.; Galeotti, F.; Muccini, M.; Toffanin, S. Organic Light-Emitting Transistors with Simultaneous Enhancement of Optical Power and External Quantum Efficiency via Conjugated Polar Polymer Interlayers. *ACS Appl. Mater. Interfaces* **2018**, *10*, 25580–25588.
- (7) Uemura, T.; Rolin, C.; Ke, T. H.; Fesenko, P.; Genoe, J.; Heremans, P.; Takeya, J. On the Extraction of Charge Carrier Mobility in High-Mobility Organic Transistors. *Adv. Mater.* **2015**, *28*, 151–155.
- (8) Bittle, E. G.; Basham, J. I.; Jackson, T. N.; Jurchescu, O. D.; Gundlach, D. J. Mobility Overestimation due to Gated Contacts in organic Field-Effect Transistors. *Nat. Commun.* **2016**, *7*, 10908.
- (9) Liu, C.; Li, G.; Di Pietro, R.; Huang, J.; Noh, Y. Y.; Liu, X.; Minari, T. Device Physics of Contact Issues for the Overestimation and Underestimation of Carrier Mobility in Field-Effect Transistors. *Phys. Rev. Appl.* **2017**, *8*, 034020.

- (10) Paterson, A. F.; Singh, S.; Fallon, K. J.; Hodsdon, T.; Han, Y.; Schroeder, B. C.; Bronstein, H.; Heeney, M.; McCulloch, I.; Anthopoulos, T. D. Recent Progress in High-Mobility Organic Transistors: A Reality Check. *Adv. Mater.* **2018**, *30*, 1801079.
- (11) Miccoli, I.; Edler, F.; Pfnür, H.; Tegenkamp, C. The 100th Anniversary of the Four-Point Probe Technique: the Role of Probe Geometries in Isotropic and Anisotropic Systems. *J. Phys. Condens. Matter.* **2015**, *27*, 223201.
- (12) Anisimov, V. I.; Aryasetiawan, F.; Lichtenstein, A. I. First-Principles Calculations of the Electronic Structure and Spectra of Strongly Correlated Systems: the LDA + U Method. *J. Phys. Condens. Matter.* **1997**, *9*, 767–808.
- (13) Pesavento, P. V.; Puntambekar, K. P.; Frisbie, C. D.; McKeen, J. C.; Ruden, P. P. Tunneling of Anyonic Majorana Excitations in Topological Superconductors. *J. Appl. Phys.* **2006**, *99*, 094504.
- (14) Alkan, M.; Yavuz, I. Intrinsic Charge-Mobility in Benzothieno[3,2-b][1]benzothiophene (BTBT) Organic Semiconductors is Enhanced with Long Alkyl Side-Chains. *Phys. Chem. Chem. Phys.* **2018**, *20*, 15970–15979.
- (15) Saito, M.; Osaka, I.; Miyazaki, E.; Takimiya, K.; Kuwabara, H.; Ikeda, M. One-Step Synthesis of [1]Benzothieno[3,2-b][1]Benzothiophene from *o*-Chlorobenzaldehyde. *Tetrahedron Lett.* **2011**, *52*, 285–288.
- (16) Combe, C. M. S.; Biniek, L.; Schroeder, B. C.; McCulloch, I. Synthesis of [1]Benzothieno[3,2-b][1]Benzothiophene Pendant and Norbornene Random Copolymers via Ring Opening Metathesis. *J. Mater. Chem. C* **2014**, *2*, 538–541.
- (17) Inoue, S.; Minemawari, H.; Tsutsumi, J.; Chikamatsu, M.; Yamada, T.; Horiuchi, S.; Tanaka, M.; Kumai, R.; Yoneya, M.; Hasegawa, T. Effects of Substituted Alkyl Chain Length on Solution-Processable Layered Organic Semiconductor Crystals. *Chem. Mater.* **2015**, *27*, 3809–3812.
- (18) Ebata, H.; Izawa, T.; Miyazaki, E.; Takimiya, K.; Ikeda, M.; Kuwabara, H.; Yui, T. Highly Soluble [1]Benzothieno[3,2-b]Benzothiophene (BTBT) Derivatives for High-Performance, Solution-Processed Organic Field-Effect Transistors. *J. Am. Chem. Soc.* **2007**, *129*, 15732–15733.
- (19) Ruzié, C.; Karpinska, J.; Sanguinet, A.; Laurent, L.; Hunter, S.; Anthopoulos, T. D.; Lemaire, V.; Cornil, J.; Kennedy, A. R.; Fenwick, O.; Samorì, P.; Schweicher, G.; Chattopadhyay, B.; Geerts, Y. H. Design, Synthesis, Chemical Stability, Packing, Cyclic Voltammetry, Ionisation Potential, and Charge Transport of [1]Benzothieno[3,2-b][1]Benzothiophene Derivatives. *J. Mater. Chem. C* **2016**, *4*, 4863–4879.
- (20) Hunter, C. A.; Sanders, J. K. M. The Nature of π - π Interactions. *J. Am. Chem. Soc.* **1990**, *112*, 5525–5534.
- (21) Vyas, V. S.; Gutzler, R.; Nuss, J.; Kern, K.; Lotsch, B. V. Optical Gap in Herringbone and π -Stacked Crystals of [1]Benzothieno[3,2-b]Benzothiophene and Its Brominated Derivative. *CrystEngComm* **2014**, *16*, 7389–7392.
- (22) Gbabode, G.; Dohr, M.; Balandier, J.; Niebel, C.; Ruzié, C.; Negrier, P.; Mondieig, D.; Geerts, Y. H.; Resel, R.; Sferrazzat, M. X-ray Structural Investigation of Nonsymmetrically and Symmetrically Alkylated [1]Benzothieno[3,2-b]Benzothiophene Derivatives in Bulk and Thin Films. *ACS Appl. Mater. Interfaces* **2014**, *6*, 13413–13421.
- (23) Izawa, T.; Miyazaki, E.; Takimiya, K. Molecular Ordering of High-Performance Soluble Molecular Semiconductors and Re-evaluation of Their Field-Effect Transistor Characteristics. *Adv. Mater.* **2008**, *20*, 3388–3392.

- (24) Inokuchi, H.; Saito, G.; Wu, P.; Seki, K.; Tang, T. B.; Mori, T.; Imaeda, K.; Enoki, T.; Higuchi, Y.; Inaka, K.; Yasuoka, N. A Novel Type of Organic Semiconductors. Molecular Fastener. *Chem. Lett.* **1986**, 1263–1266.
- (25) Nan, G.; Li, Z. Crystal Structure versus Charge Transport in Organic Single Crystals of [1]Benzothieno[3,2-b][1]benzothiophene Derivatives from a Multiscale Theoretical Study. *J. Mater. Chem. C* **2014**, *2*, 1447–1456.
- (26) Minemawari, H.; Tsutsumi, J.; Inoue, S.; Yamada, T.; Kumai, R.; Hasegawa, T. Crystal Structure of Asymmetric Organic Semiconductor 7-Decyl-2-phenyl[1]Benzothieno[3,2-b][1]Benzothiophene. *Appl. Phys. Express* **2014**, *7*, 091601.
- (27) Marinov, O.; Deen, M. J.; Zschieschang, U.; Klauk, H. Organic Thin-Film Transistors: Part I-Compact DC Modeling. *IEEE Trans. Electron Devices* **2009**, *56*, 2952–2961.
- (28) Marinkovic, M.; Belaineh, D.; Wagner, V.; Knipp, D. On the Origin of Contact Resistances of Organic Thin Film Transistors. *Adv. Mater.* **2012**, *24*, 4005–4009.
- (29) Choi, H. H.; Rodionov, Y. I.; Paterson, A. F.; Panidi, J.; Saranin, D.; Kharlamov, N.; Didenko, S. I.; Anthopoulos, T. D.; Cho, K.; Podzorov, V. Accurate Extraction of Charge Carrier Mobility in 4-Probe Field-Effect Transistors. *Adv. Funct. Mater.* **2018**, *28*, 1707105.
- (30) van der Pauw, L. J. A Method of Measuring the Resistivity and Hall Coefficient on Lamellae of Arbitrary Shape. *Philips Tech. Rev.* **1958**, *20*, 220–224.
- (31) van der Pauw, L. J. A Method of Measuring Specific Resistivity and Hall Effect of Disks of Arbitrary Shape. *Philips Res. Rep.* **1958**, *13*, 1–9.
- (32) Rolin, C.; Kang, E.; Lee, J.-H.; Borghe, G.; Heremans, P.; Genoe, J. Charge carrier Mobility in Thin Films of Organic Semiconductors by the Gated van der Pauw Method. *Nat. Commun.* **2017**, *8*, 14975.
- (33) Dhoot, A. S.; Wang, G. M.; Moses, D.; Heeger, A. J. Voltage-Induced Metal-Insulator Transition in Polythiophene Field-Effect Transistors. *Phys. Rev. Lett.* **2006**, *96*, 246403.
- (34) Dhoot, A. S.; Aramaki, S.; Moses, D.; Heeger, A. J. Metal-Insulator Transition in Solution-Processible Porphyrinic Field-Effect Transistors. *Adv. Mater.* **2007**, *19*, 2914–2917.
- (35) Kang, E. S. H.; Kim, E. Multi-Barrier Field-Emission Behavior in PBTTT Thin Films at low temperatures. *Sci. Rep.* **2015**, *5*, 8396.
- (36) Yuen, J. D.; Menon, R.; Coates, N. E.; Namdas, E. B.; Cho, S.; Hannahs, S. T.; Moses, D.; Heeger, A. J. Nonlinear Transport in Semiconducting Polymers at High Carrier Densities. *Nat. Mater.* **2009**, *8*, 572–575.
- (37) He, D.; Qiao, J.; Zhang, L.; Wang, J.; Lan, T.; Qian, J.; Li, Y.; Shi, Y.; Chai, Y.; Lan, W.; Ono, L. K.; Qi, Y.; Xu, J. B.; Ji, W.; Wang, X. Ultrahigh Mobility and Efficient Charge Injection in Monolayer Organic Thin-Film Transistors on Boron Nitride. *Sci. Adv.* **2017**, *3*, e1701186.
- (38) Bourbie, D. Field-Induced Crossover from Phonon to Field Assisted Hopping Conductivity in Organic Materials. *Appl. Phys. Lett.* **2011**, *98*, 012104.
- (39) Ikrelef, N.; Bourbie, D.; Driss-Khodja, K. On the Inverse Field Dependence of Conductivity in Disordered Organic Materials. *Appl. Phys. Lett.* **2010**, *97*, 022101.
- (40) Bourbie, D.; Ikrelef, N.; Driss-Khodja, K.; Nedellec, P. Temperature- and Field-Dependent Conductivity in Disordered Materials. *Phys. Rev. B Condens. Matter Mater. Phys.* **2007**, *75*, 184204.